Reprinted from The Journal of Physical Chemistry, 1990, *94*, 737.
Copyright © 1990 by the American Chemical Society and reprinted by permission of the copyright owner.

Excitonic Interactions in Naphthalene Clusters

John E. Wessel* and Jack A. Syage

The Aerospace Corporation, P.O. Box 92957, Los Angeles, California 90009 *(Received: June 5, 1989)*

Well-resolved vibronic spectra, recorded by resonance two-photon ionization, are analyzed for cold naphthalene cluster species. Spectra for isotopically pure tetramers and both pure and mixed isotopic trimer clusters provide information on resonant (excitonlike) interactions. An analysis of the spectra suggests that the tetramer geometry resembles bulk crystalline naphthalene, whereas the trimer structure minimizes direct contact interactions. Cluster geometry is similar in ground and excited states of these clusters and there is no direct evidence for rapid dynamics in the excited states, nor is there evidence of multiple geometric conformations. Analysis of the isotopically mixed trimers suggests a preference for the HDH conformation, rather than HHD. An empirical weak interaction model provides a successful descripton of the observed spectra. Excitonic splittings are approximately proportional to dipole transition strengths for the vibronically induced spectra, whereas low-intensity allowed origin transitions exhibit splittings that greatly exceed dipolar contributions. Both results indicte that the long-range intermolecular potential exceeds simple estimates. This method of analysis may be applicable to studies of larger clusters, providing new information on size-dependent structure and dynamics.

I. Introduction

Elegant low-temperature spectroscopic studies of organic molecular crystals provided a detailed description of resonant intermolecular interactions (excitons) in molecular crystals.[1-6] Supersonic molecular beam technology now makes it possible to study these interactions for cold, isolated cluster molecules. In a previous paper[7] we presented qualitative evidence for excitionic interactons in naphthalene trimer and tetramer clusters. In this report we present and analyze new spectra, including those for isotopic mixed clusters, which provide the basis for a quantitative treatment of excitonic interactions in the clusters.

Molecular cluster spectroscopy provides an ideal probe of resonance interactions because translationally equivalent interactions and dielectric effects are eliminated. In analogy to the crystal studies, it is possible to analyze the cluster spectra in terms of moderately weak pairwise interactions between monomer species embedded in the clusters, as shown in Figure 1. We find that a simple model of pairwise interaction between monomer units, each with an independent transition moment, provides predictions in reasonable agreement with experimental results. It is clear from the well-resolved spectra that excitonic interactions dominate the specta, and there is no clear evidence of conformers or rapid dynamical effects for the trimer or tetramer. Inequivalent site interactions are not evident in the trimer spectra, whereas they are clearly present for the tetramer.

Crystalline naphthalene is a particularly well-studied system. Hanson[6] directly measured the pairwise interactions between naphthalene molecules in the S_1 state by studying isotopic mixed crystals, in which interactions between pairs of guest molecules are isolated from the resonant interactions of the host crystal exciton bands. In crystalline system, translationally equivalent interactions form extended bands of exciton states. The characteristic discrete exciton components (Davydov splitting) observed in these spectra arise from selection rules that restrict transitions to exciton states with crystal momentum ($\vec{k}$) near zero. The multiple discrete components arise from symmetrically inequivalent sites or interchange equivalent sites within the unit cell. However, the interactions contributing to these splittings extend over the entire crystal. Hanson's work was particularly significant because it allowed the complex overall exciton band structure to be understood in terms of directly measured local pairwise intermolecular interactions. The crystal studies were limited to the origin system due to total absorption at shorter wavelengths. However, the vibronic transitions were not considered interesting because exciton theory[2-5] for weak interactions suggested that excitonic splitting is limited to the origin and totally symmetric vibrational additions.

Previously, discrete spectra were observed for benzene dimers[8-10] and in the chemical dimer spectra of cold binaphthyl molecules, as reported by Jonkman and Wiersma,[11] and for larger benzene clusters formed in a supersonic beam, as reported by Hopkins, Powers, and Smalley.[12] Recently, Bornsen, Lin, Selzle, and Schlag studied isotopically mixed benzene trimers, clearly resolving two isotopic conformations with important intermolecular vibrational structure.[13] Their analysis of the excitonic features supports a zigzag structure for the cluster. Many other dimer and cluster systems display strong evidence of conformers or have broadened spectra suggesting the occurrence of rapid dynamical processes, including excimer formation in solution and in chemically bonded dimers such as naphthalene paracyclophanes, which were reviewed by Ferguson.[14]

The structure and dynamics of large isolated molecular clusters is currently the subject of considerable scientific interest. In particular, Easter, El-Shall, Hahn, and Whetten[15] report complex spectral structure for benzene clusters ranging in size to $n > 16$. Discrete sharp structure becomes less evident as cluster size increases from $n = 5$ to $n = 9$; however, the bands sharpen substantially by $n = 13$. They observe complex sharp multiplet structure from $n = 13$ to $n = 16$. This is interpreted in terms of the shell structure model, in which a shell is closed at $n = 13$, resulting in high site symmetry for molecules in the cluster. The temperature dependence of the spectra suggests the onset of phase transformation processes. In the case of the naphthalene van der Waals trimer and tetramer discussed below, the unique relationship between vibronic species and transition moment direction provides direct information which is used to determine cluster geometry and furnishes considerable information concerning intermolecular

(1) Robinson, G. W. *Annu. Rev. Phys. Chem.* **1970**, *21*, 429.
(2) Craig, D. P.; Walmsley, S. H. *Excitons in Molecular Crystals*; Benjamin: New York, 1968.
(3) Hochstrasser, R. M. *Annu. Rev. Phys. Chem.* **1966**, *17*, 457.
(4) Knox, R. S. *Theory of Excitons*; Academic Press: New York, 1963.
(5) Davydov, A. S. *Theory of Molecular Excitons*; Translated by M. Kasha and M. Oppenheimer, Jr.; McGraw-Hill: New York, 1962.
(6) Hanson, D. M. *J. Chem. Phys.* **1970**, *52*, 3409.
(7) Syage, J. A.; Wessel, J. E. *J. Chem. Phys.* **1988**, *89*, 5962.
(8) Bornsen, K. O.; Selzle, H. L.; Schlag, E. W. *J. Chem. Phys.* **1986**, *85*, 1726.
(9) Wanna, J.; Menapace, J. A.; Bernstein, E. R. *J. Chem. Phys.* **1986**, *85*, 77.
(10) Law, K. S.; Schauer, M.; Bernstein, E. R. *J. Chem. Phys.* **1984**, *81*, 4871.
(11) Jonkman, H. T.; Wiersma, D. A. *Chem. Phys. Lett.* **1983**, *97*, 261.
(12) Hopkins, J. B.; Powers, D. E.; Smalley, R. E. *J. Chem. Phys.* **1981**, *85*, 3739.
(13) Bornsen, K. O.; Lin, S. H.; Selzle, H. L.; Schlag, E. W. *J. Chem. Phys.* **1989**, *90*, 1299.
(14) Ferguson, J. *Chem. Rev.* **1986**, *86*, 957.
(15) Easter, D. C.; El-Shall, M. S.; Hahn, M. Y.; Whetten, R. L. *Chem. Phys. Lett.* **1989**, *157*, 277.

0022-3654/90/2094-0737$02.50/0 © 1990 American Chemical Society

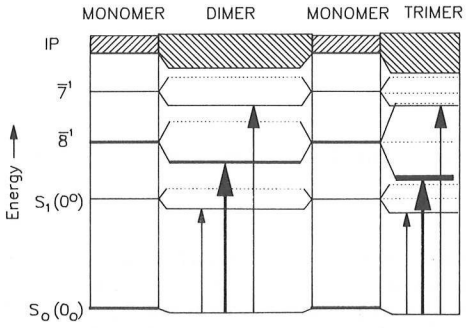

Figure 1. Energy-level diagram representing the spectra of the monomer, dimer, and trimer clusters. In the dimer, each pair of monomer vibronic levels generates a pair of dimer components. In the dipole interaction approximation, the separation of components is proportional to the dipole intensity of the transition. Intense transitions are denoted by thick lines.

interactions. Eventually, it may be possible to extend this type of analysis to the larger systems of current interest.[15]

II. Experimental Section

A conventional differentially pumped pulsed molecular beam apparatus was used in conjunction with a time-of-flight mass spectrometer.[16] The valve was based on a temperature-controlled magnetic solenoid design. Typical expansion conditions were 50 psi He flowing over naphthalene maintained at about 80 °C. The nozzle diameter was 0.5 mm. Mixed isotopic species were produced by mixing the solid naphthalene introduced into the pulsed valve sample chamber. Signals were recorded by using gated time of flight mass detection, and the output was digitized and stored as a function of excitation wavelength.

A frequency doubled pulsed dye laser provided excitation. A home-built phase-angle autotracking device was employed to maintain efficient frequency doubling during wavelength scans. The dye laser was excited by a frequency doubled, pulsed Nd:YAG laser. The ultraviolet excitation pulse, of 10–100 μJ energy with a duration of approximately 5 ns, was focused into the collimated region of the supersonic beam by a 30 cm focal length lens. The reported spectra are uncorrected for variation in laser beam intensity with wavelength. Expansion conditions and laser beam intensity were adjusted so as to minimize interfering signals contributed by fragmentation of clusters larger than the species of interest. The excess ionization energy imparted to naphthalene clusters by (1 + 1) ionization is believed to range from about 0 to 1000 cm^{-1} for the trimer and tetramer. This is substantially less than the anticipated cluster ion dissociation energies and is consistent with the observed absence in each spectrum (recorded at a particular ion mass) of discrete spectral features associated with larger cluster ions. Only when excitation intensity is increased signficantly do spectral features corresponding to fragmentation of larger cluster ions appear. In the case of naphthalene, these are easily identified by their characteristic spectral features.

III. Background

A. Naphthalene Monomer Spectrum. Geometric information is available from the naphthalene cluster spectra because the excitonic interactions are strongly dependent on the angle of the transition moments of monomer units of the cluster. In favorable cases, the geometry can be determined if a single transition moment gives rise to a spectral feature of the cluster. Naphthalene is highly favorable for this analysis because there are two separate transition moments in the S_1–S_0 transition system. The weak origin and a_g mode system are long axis polarized, and the stronger vibronically induced b_{3g} system is short axis polarized. In principle, an analysis of the splittings and intensities of the cluster transitions can provide the angular orientation of the monomers within the clusters, and more detailed structural information can be obtained by applying a model of the intermolecular interaction potential. Whereas unique and accurate geometries may not result from this

(16) Syage, J. A.; Wessel, J. E. *J. Chem. Phys.* **1987**, *87*, 3313.

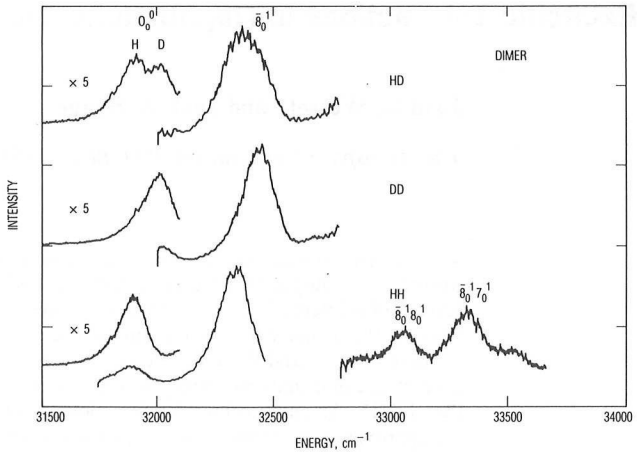

Figure 2. Spectra of isotopically pure (HH, DD) and mixed (HD) naphthalene dimer species.

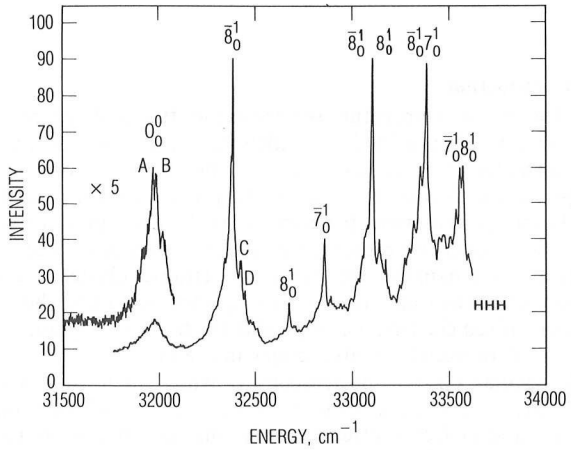

Figure 3. Spectrum of the HHH trimer.

treatment, the analysis can rule out a large class of geometries.

The adiabatic ionization potential of naphthalene[17] is 65 666 cm^{-1}, which implies a threshold for two-photon ionization of 32 833 cm^{-1}. Therefore, the vibronic band $b_{3g}(7)$ (denoted $\bar{7}_0^1$), at 32 931 cm^{-1}, is the first transition in the spectrum of the lowest excited singlet state (S_1) accessible by two-photon ionization (refer to Table I). The ionization spectrum obtained in a supersonic beam is well documented through the work of Smalley and co-workers.[18] It closely resembles the fluorescence excitation spectrum,[18,19] which more directly reflects one-photon absorption. The fluorescence excitation spectrum reveals lower energy transitions, starting at the weak origin (32 020 cm^{-1}). A gap follows, with virtually no observable transitions, and then an intense vibronically induced transition appears at +435 cm^{-1}, designated by $b_{3g}(8)$ vibrational symmetry (denoted $\bar{8}_0^1$ in the nomenclature of Stockburger et al.[19]). The origin transition is polarized along the long molecular axis and $\bar{8}_0^1$ is short axis polarized, as revealed by high-resolution rotational analysis in the vapor[20] and by studies on mixed crystal systems at low temperature.[21,22] Transition strength for $\bar{8}_0^1$ derives principally from interaction with the S_2 state, induced by the vibrational deformation. There are weak long axis polarized transitions at higher energy, such as $a_g(8)$ (denoted 8_0^1) at +702 cm^{-1}. However, the higher energy spectrum is dominated by b_{3g}

(17) Duncan, M. A.; Dietz, T. G.; Smalley, R. E. *J. Chem. Phys.* **1981**, *75*, 2118.
(18) Beck, S. M.; Powers, D. E.; Hopkins, J. B.; Smalley, R. E. *J. Chem. Phys.* **1980**, *73*, 2019.
(19) Stockburger, M.; Gattermann, H.; Klusmann, W. *J. Chem. Phys.* **1975**, *63*, 4519; **1975**, *63*, 4529.
(20) Craig, D. P.; Hollas, J. M.; Redies, M. F.; Wait Jr., S. C. *Philos. Trans. R. Soc.* **1961**, *A253*, 543; **1961**, *A253*, 569.
(21) McClure, D. S. *J. Chem. Phys.* **1954**, *22*, 1668.
(22) Wessel, J. "Degenerate Vibronic Interference in Naphthalene"; Dissertation, University of Chicago, Chicago, 1970.

TABLE I

Monomer, h_8

assignt	energy, cm^{-1}	assignt	energy, cm^{-1}
$0,0^a$	32020	$\bar{8}^1,9^1$	936
$\bar{8}^{1\,b}$	+435	7^1	987
$9^{1\,c}$	501	$\bar{8}^1,8^1$	1137
$8^{1\,c}$	702	$\bar{8}^1,7^1$	1422
$\bar{7}^{1\,b}$	911		

Monomer, d_8

assignt	energy, cm^{-1}	assignt	energy, cm^{-1}
0,0	32138	$\bar{7}^1$	819
$\bar{8}^1$	+418	$\bar{8}^1,8^1$	1055
8^1	637		

Dimer, HH

assignt	energy, cm^{-1}	$\Delta\bar{\lambda}$, cm^{-1}	fwhm, cm^{-1}
$0,0^d$	31883		128
$\bar{8}^1_0$	32315	432	160
$\bar{7}^1_0$	32800	917	
$\bar{8}^1_0,8^1_0$	33040	1157	109
$\bar{8}^1_0,7^1_0$	33314	1431	147

Dimer, HD

assignt	energy, cm^{-1}	$\Delta\bar{\lambda}$, cm^{-1}
$0,0,H^d$	31895	
0,0, D	31988	
$\bar{8}^1_0$	32347	452

Dimer, DD

assignt	energy, cm^{-1}	$\Delta\bar{\lambda}$, cm^{-1}	fwhm, cm^{-1}
$0,0^d$	31995		164
$\bar{8}^1_0$	32419	424	152

Pentamer, HHHHH

assignt	obsd energy, cm^{-1}	$\Delta\bar{\lambda}$, cm^{-1}
0,0	31883	
$\bar{8}^1_0$	32276	394

[a] From ref 17. [b] The $b_{3g}(8)$ mode is denoted $\bar{8}^1$, and $b_{3g}(7)$ by $\bar{7}^1$. [c] The $a_g(9)$ mode is denoted by 9^1, the $a_g(8)$ mode by 8^1, etc. [d] The origin band-center frequency is reported. The actual origin may be 100 cm^{-1} or more to the red if excimer interaction occurs.

symmetry combination vibronic transitions, such as $\bar{8}^1_0$, 8^1_0 at 1137 cm^{-1}, $\bar{8}^1_0$, 7^1_0 at 1422 cm^{-1}, and by $\bar{7}^1_0$ at 911 cm^{-1}, and its combinations with a_g modes. These spectroscopically observable states provide a basis set of zero-order levels which are applicable to the analysis of excitonic interactions in the cluster spectra.

B. Ionization of Dimer and Larger Clusters. The ionization potential is altered in the clusters. We observe strong resonance two-photon ionization at $\bar{8}^1_0$ for the dimer (Figure 2) and for larger clusters (Figures 3 and 4), whereas in the monomer, $\bar{8}^1_0$ is exceedingly weak because it is below the (1 + 1) ionization limit. The origin transitions in the clusters are weaker than $\bar{8}^1_0$ by an order of magnitude, probably due to the low oscillator strength of the ground-state transition. However, it is possible that three-photon excitation is required, or that the ionizing transition is weak, due to small Franck–Condon factors for an intermolecular vibrational mode. We attempted to measure ionization potentials for clusters by resonantly exciting the origin transitions and then inducing ionization with a second laser beam, which is scanned across the ionization thresholds. No sharp thresholds were observed for the dimer, and the signal-to-noise ratios were insufficient to draw conclusions for larger species. The dimer results imply either that geometry changes significantly between the S_1 dimer state and the ion, such that a long progression is observed in a low energy intermolecular vibrational mode, or that the S_1 dimer state is unstable.

C. Model for Resonance Interactions. Representative spectra for naphthalene dimer, trimer, and tetramers are presented in Figures 2–4. The basic vibrational structure resembles the monomer spectrum, with the exceptions that considerable broadening occurs for the dimer, and multiplet structure appears in transitions of the larger clusters. Nonetheless, it is easy to identify each spectral band (multiplet) of a cluster and associate it with the corresponding vibronic transition of the monomer. For the trimer, we observe two principal components for the origin and single principal components for the vibronic transitions. The tetramer has a single principal origin component and four components appear in the vibronic transitions.

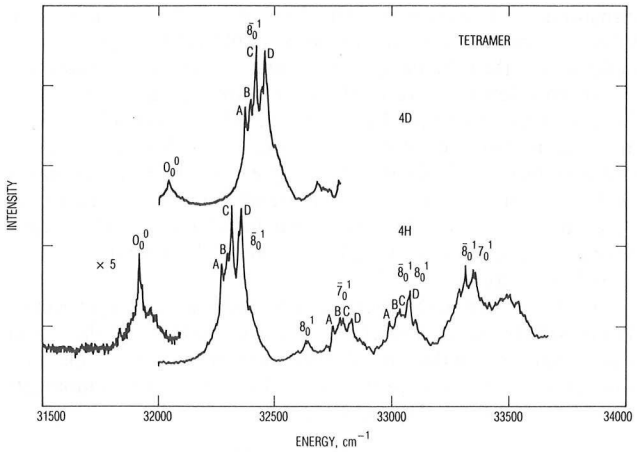

Figure 4. Spectra of the HHHH and DDDD tetramer clusters.

This suggests that the trimer and tetramer spectra can be described by a weak interacton model, in which the dominant intermolecular interactions consist of the resonant terms connecting similar vibronic excitations on nearby monomers. The block factored Hamiltonian matrix for a single vibronic state of the monomer is given by

$$H = \begin{pmatrix} \epsilon_{11} & H_{12}\cdots H_{1n} \\ H_{21} & \epsilon_{22}\cdots H_{2n} \\ H_{n1} & \cdots\epsilon_{nn} \end{pmatrix} \tag{1}$$

where n is the number of monomer units and ϵ_{ii} represents the ith site shifted (vibronic) energy attributable to the symmetry inequivalent nonresonant intermolecular interactions. In the Results section below, we use the term band center to describe the experimentally estimated zero-order energies (site and resonance interaction free). Off-diagonal terms, H_{ij}, describe resonance interactions between monomer units. These can be approximated analytically, by a multipolar expansion, or can be supplied as empirical parameters. In the adiabatic approximation, interaction matrix elements can be expressed as

$$\langle H_{ij}\rangle = \langle X_i^*|\langle X_j|\langle\psi_i^*|\langle\psi_j|V_{ij}|\psi_i\rangle|\psi_j^*\rangle|X_i\rangle|X_j^*\rangle \tag{2}$$

where ψ_n is the electronic wave function of molecule n, the * denotes excitation, the vibrational wave function of molecule n is X_n, and the interaction operator is given by

$$V_{ij} = (e^2\mu_i\mu_j/R_{ij}^3)(\mathbf{m}_i\cdot\mathbf{m}_j - 3(\mathbf{m}_i\cdot\mathbf{r}_{ij})(\mathbf{m}_j\cdot\mathbf{r}_{ij}))$$

where e is the electric charge, μ_i is the magnitude of the transition moment associated with the vibronic state of molecule i, R_{ij} is the distance between molecules i and j, $\mathbf{m}_i$ is a unit vector in the direction of the transition moment, and $\mathbf{r}_{ij}$ is a unit vector connecting molecules i and j.

In the Condon approximation, the vibrational and electronic matrix elements are taken to be independent, therefore the vibrational overlap terms are factored from eq 2, resulting in

$$H_{ij} = H_{ij}^{el}\langle X_i^*|X_i\rangle\langle X_j|X_j^*\rangle$$

where H_{ij}^{el} is the electronic matrix element. The vibrational overlap integrals vanish for change in quanta, except between Franck–Condon active modes, and the electronic term is identical with the product of transition moment operators for the two molecules in question. Thus, the interaction terms should be proportional to the intensity of the corresponding molecular

transition, to the extent that the dipolar approximation is valid. Vibronic activity in b_{3g} modes of S_1 naphthalene represent deviations from the Condon approximation. In this case, the observed transition intensities are used to calculate dipolar interactions. (The weak coupling case discussed here differs qualitatively from the case of strong excitonic coupling, in which intermolecular interactions exceed vibrational energies. In the latter case, the electronic transitions split into separate excitonic components, each characterized by unsplit vibrational manifolds. This requires resonance interactions exceeding 1000 cm^{-1}, beyond the range considered here.)

Diagonalization of the energy matrix yields a set of eigenvectors that provide transition intensities. The basis function for the cluster is approximated, in the case of weak interactions, as a single-term product of monomer wave functions. Cluster transition moments are calculated from the vector sum

$$\mathbf{M}_i = \sum_{j=1,n} (c_{ij}\mathbf{m}_j)M_j \qquad (3)$$

of monomer transition moments, weighted by the excited-state coefficients, as in eq 3. Intensities are calculated by squaring these sums and adding together contributions from each orthogonal polarization direction. The relative orientation of monomer transition moment directions must be supplied to the calculations; however, relative positions (molecular centers) are not required (except to calculate dipolar interaction energies). In the case of naphthalene, high-symmetry geometries can be ruled out, based on group theoretical predictions, as described in a following section. Intensity calculations are far more informative and they are readily performed as a function of interaction parameters and monomer orientations. (Typical results for the trimer and tetramer are presented in the following section.) Two general features of the calculations warrant mention. The center of gravity of the components remains unchanged by the interactions and the resonance interactions dominate the spectra when the site shifts are small, resulting in fewer prominent components than are otherwise expected.

For parallel monomer transition moments in the absence of site splitting, one cluster component receives predominant intensity. If the resonance interactions are negative (stabilizing), the lowest energy component carries all intensity. If interactions are positive (repulsive), only the highest energy component is observed. Although the real system is expected to be more complex, with pairwise interactions varying from positive to negative, spectra for several vibronic transitions of the clusters consist of isolated single components, in accord with the simple model. When the transition moments are nonparallel, additional components become observable. In the case of naphthalene, the interaction energies can be deduced from the spectra. The angular orientation of transition moments are obtained by varying the input angles in the calculation, until a match is achieved between calculated and observed intensities. In this simplified model, the relative intensities of components within each vibronic band of the same symmetry should be similar from band to band, provided site shifts are small, because the ratios between interaction matrix elements, which control the intensity distribution, remain the same, although the overall magnitudes of the interactions change from vibration to vibration. This is based on the weak interaction model which allows cluster states to be represented by the product of monomer wave functions. If this case holds, spectra of the isotopically pure proto- and deuteroclusters will resemble each other. In the absence of vibronic coupling, resonance interactions involving nontotally symmetric vibrational excitations should vanish as a consequence of orthogonal vibrational overlap integrals. In this approximation, excitonic splitting will occur only for the origin and a_g levels, with the magnitude of the splitting proportional to the Franck–Condon factor of the vibrational level. For the case of naphthalene, vibronic coupling complicates this description. If the interactions are primarily dipolar interaction, the coupling should scale in proportion to the intensity of the vibronic transition. Again, the spectra of isotopically pure clusters should be similar if the monomer spectra are similar. In this approximation the $\bar{8}^1$ level should display maximum resonance interaction, and dipolar splitting in the origin should be an order of magnitude smaller.

TABLE II: Pairwise Dipolar Interaction Energy (cm^{-1}) for $\bar{8}_0^1$ in the Trimer[a]

R, Å	monomer[b] parameters	solvent[c] enhanced	solvent and[d] Franck–Condon enhanced
5	−1.6	−1.9	−3.8
4.5	−2.2	−2.6	−5.2
4	−3.1	−3.7	−7.4
3.5	−4.6	−5.5	−11.0
3	−7.3	−8.8	−17.5

[a] Assuming trimer geometry with parallel transition moments lying along a line connecting the molecules. [b] The monomer transition dipole moment is assumed to be 0.14 D. [c] Calculation based on the treatment of Liver et al., using the shift of $\bar{8}_0^1$ from monomer to trimer, with the transition moments parallel to the intermolecular axis. [d] Assuming the Franck–Condon factor for $\bar{8}_0^1$ is enhanced by a factor of 2 in the trimer.

The transition moment for the naphthalene $\bar{8}_0^1$ transition is required in order to apply the dipolar interaction model. This can be calculated on the basis of the radiative lifetime for the monomer $\bar{8}^1$ level, extrapolated to collisionless conditions,[23] combined with the fractional integrated intensity of the $\bar{8}_0^1$ transition[24] (we estimate this to account for 0.16 of total S_1–S_0 intensity). This yields a transition moment of 0.14 D. The corresponding maximum dipole–dipole interacton energy at the crystal intermolecular separation of 5 Å is ±1.6 cm^{-1}, which is substantially less than the interactions observed in trimer and tetramer spectra. Larger values are obtained at reduced intermolecular distances, and solvent-type dielectric effects extended to clusters by Liver, Nitzan, Amirav, and Jortner[25] can provide additional enhancement for the trimer. Table II presents estimates for dipolar interactions in the presence of solvent enhancement, based on the observed shifts of transition energies from monomer to trimer, for a trimer with monomer transition moments aligned parallel to the intermolecular axes. The values are tabulated for several intermolecular separation distances, and for the case in which the Franck–Condon factor of the trimer $\bar{8}_0^1$ transition is twice that of the monomer. The observed spectra are best described by the larger estimates for dipolar interactions; therefore in the following analyses we assume the appropriate interaction for $\bar{8}_0^1$ is approximately 10 cm^{-1} (e.g., =0.23 D, R = 3.8 Å).

In the discussions below, the interaction matrix elements are expressed as H_{12}, H_{23}, H_{13}, etc., where the first two represent the strongest pairwise interactions, presumably between nearest neighbors. Site shifts should be the same for each vibrational level. Therefore, they can be estimated by comparison of the positions of corresponding components for different vibrational transitions. (A more refined approach might be based on a Green's function analysis.)

IV. Results and Discussion

A. Dimer. The dimer spectra are characterized by broad, asymmetric bands. Vibrational frequencies derived from band center positions are essentially identical with monomer vibrational frequencies, as indicated in Table I. The origin red shift is substantial, suggesting the dimer may transform into excimer geometry in S_1, such that the broadening arises from an unresolved progression in low-energy intermolecular vibrations. In this case, the origin transition will be far below the peak transition energy reported in Table I. Nonetheless, the mixed isotope dimer spectrum, shown in Figure 2, reveals separate bands corresponding to h_8 and d_8 monomer units of the cluster. These are essentially unshifted in energy relative to the pure isotopic dimers. Similar isotopic shift behavior was previously reported for benzene dimers by Bornsen, Selzle, and Schlag.[8] These authors suggested that unshifted transition energies for isotopic components in both pure

(23) Behlen, F. M.; Rice, S. A. *J. Chem. Phys.* **1981**, *75*, 5672.
(24) Beck, S. M.; Hopkins, J. B.; Powers, D. E.; Smalley, R. E. *J. Chem. Phys.* **1981**, *74*, 43.
(25) Liver, N.; Nitzan, A.; Amirav, A.; Jortner, J. *J. Chem. Phys.* **1988**, *88*, 3516.

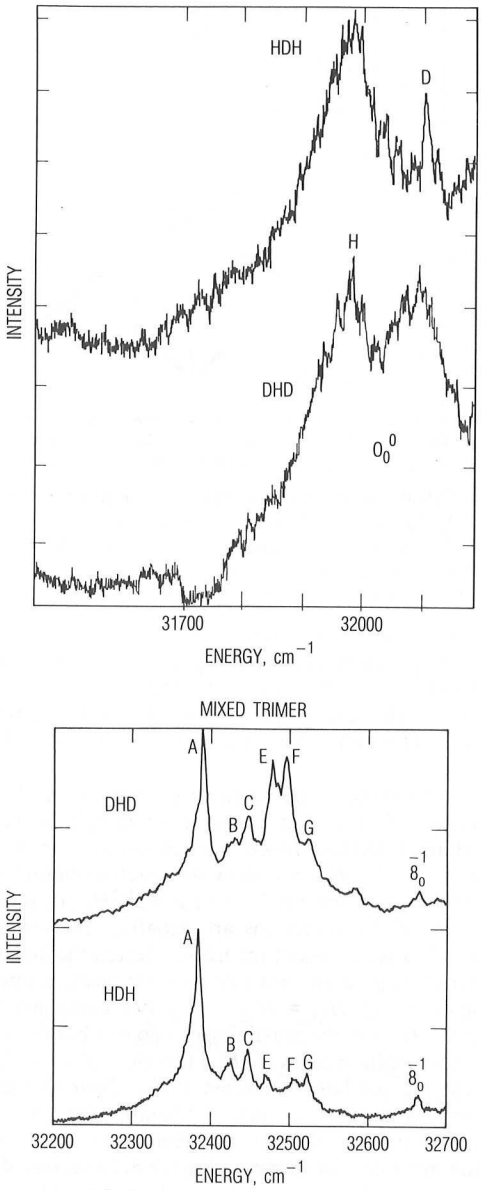

Figure 5. Spectra of the DHD and HDH trimers in (a, top) the origin region, and (b, bottom) the region of $\bar{8}_0^1$. The letters in (b) designate corresponding components.

and mixed clusters imply that a localized exciton model is appropriate for the dimer.

B. Trimer. 1. Trimer Spectra. Spectra of the trimer species HHH, HDH, and DHD are represented in Figures 3 and 5, and Table III summarizes transition energies. Prominent sharp transitions appear at energies corresponding to the monomer origin, $\bar{8}_0^1$, 8_0^1, $\bar{7}_0^1$, and combination transitions. The absence of promient multiplet structure for most of the vibrational modes suggests that there is only one conformer and that site inequivalent interactions are small and do not exceed the spectral resolution, thus supporting the assignment of multiplet structure to resonance interaction. In the discussion of resonance interactions below, we explore the implications of a doublet origin for HHH and DDD, together with single components for nontotally symmetric modes $\bar{8}^1$ and $\bar{7}^1$. Spectra for HHH and DDD are essentially identical, except that vibrational frequencies are shifted, as noted in Table III. (No splitting is observed for the totally symmetric 8^1 mode, probably as a result of reduced resonance interactions.) For the pure isotopic species, the vibronic transitions shown are single sharp peaks, with a substantial intensity pedestal for most transitions. The pedestal includes minor peaks (C) and (D) in Figure 3 located on the high-energy side of the principal transitions, presumably corresponding to intermolecular vibrations. Their low intensity, relative to the principal components, implies that the trimers do not change geometry significantly between the ground and excited state.

There are at least three possible starting assumptions for a vibrational analysis of the trimer S_1 spectra. (1) The trimer could have a C_3 symmetry element, which implies equivalence of sites, thus explaining the lack of observed site splitting, or symmetry

TABLE III

Trimer, HHH

assignt	obsd energy, cm^{-1}	$\Delta\bar{\lambda}$, cm^{-1}	$\Delta\bar{\lambda}$(trimer) − $\Delta\bar{\lambda}$(monomer)[b]
0,0, A	31 953	−12	
0,0[a]	31 965	0	
0,0, B	31 967	2	
0,0 + v	32 008	43	
$\bar{8}_0^1$	32 368	403	−32
$\bar{8}_0^1$ + v C	32 411	446	
8_0^1	32 656	691	−11
$\bar{7}_0^1$	32 841	876	−35
$\bar{7}_0^1$ + v	32 874	909	
$\bar{8}_0^1,8_0^1$	33 085	1120	−17
$\bar{8}_0^1,8_0^1$ + v	33 121	1156	
$\bar{8}_0^1,8_0^1$ + v′	33 154	1189	
$\bar{8}_0^1,7_0^1$	33 366	1411	−21
$\bar{7}_0^1,8_0^1$	33 555	1600	−23

Trimer, DDD

assignt	obsd energy, cm^{-1}	$\Delta\bar{\lambda}$, cm^{-1}	$\Delta\bar{\lambda}$(trimer) − $\Delta\bar{\lambda}$(monomer)[b]
0,0, A	32 069	−14	
0,0 band center[a]	32 083		
0,0, B	32 085	2	
$\bar{8}_0^1$	32 472	389	−29
$\bar{8}_0^1$ + v G	32 513	430	
8_0^1	32 702	619	−18
$\bar{7}_0^1$	32 863	780	−39

Trimer, DHD

assignt	obsd energy, cm^{-1}	zero-order energy, cm^{-1}	zero-order $\Delta\bar{\lambda}$, cm^{-1}
0,0[c]	31 964	31 966[e]	
$\bar{8}_0^1$, A	32 372	32 379	413
$\bar{8}_0^1$, B	32 412		
$\bar{8}_0^1$, C	32 430		
$\bar{8}_0^1$, E	32 461		
$\bar{8}_0^1$, F	32 478	32 479[d]	
$\bar{8}_0^1$, G	32 505		
8_0^1	32 644	32 644	678

Trimer, HDH

assignt	obsd energy, cm^{-1}	zero-order energy, cm^{-1}	zero-order $\Delta\bar{\lambda}$, cm^{-1}
0,0[f]	31 963	31 967[i]	
0,0[g]	32 090	32 088	
$\bar{8}_0^1$, A	32 368	32 378	411
$\bar{8}_0^1$, B	32 410		
$\bar{8}_0^1$, C	32 431		
$\bar{8}_0^1$, E	32 456		
$\bar{8}_0^1$, F	32 490	32 483[h]	
$\bar{8}_0^1$, G	32 507		
8_0^1	32 649		682
$\bar{8}_0^1,8_0^1$	33 077		1112

[a] Origin band center (not observed), position estimated from resonance calculation. [b] Shift from monomer vibrational energy, partly due to resonance interaction. [c] Component corresponding to H. [d] Estimated position of $\bar{8}_0^1$ for the zero-order D molecules, given by 31 966 cm^{-1} plus the isotope shift of 118 cm^{-1} plus the trimer D vibrational frequency of 395 cm^{-1}. [e] Corrected for −2 cm^{-1} shift due to the H molecule interacting with D molecules. [f] Component corresponding to H. [g] Component corresponding to D. [h] Zero-order D origin + 395 ($\bar{8}^1$ for D). [i] Corrected for the HH interaction.

could be lower with a geometry that minimizes site inequivalent interactions, and (2) vibrational analysis could be based on the assumption of unperturbed vibrational frequencies for the weakly coupled vibrational modes, or (3) the vibrational analysis could be based on an origin band center deduced from the isotopic mixed cluster spectra. These approaches lead to different conclusions concerning trimer geometry and intermolecular interactions. We adopt the third choice because it is uniquely consistent with the mixed isotope spectra and with the requirements imposed by dipolar intermolecular interactions involving the strong vibronic transitions. These issues are discussed extensively below.

Based on this assumption, the isotopically pure clusters display excitonic behavior, with an origin doublet splitting of 16 cm^{-1} (peaks A and B), which represents resonance interaction between naphthalenes within the cluster. The large splitting is inconsistent with high-symmetry cluster geometries (C_3), for which group theory predicts a degenerate pair of allowed transitions. The mixed isotope origin spectra of DHD and HDH in Figure 5 provide an excellent basis to estimate the origin band centers in DDD and HHH, corresponsing to resonance interaction free conditions. The H component of DHD (31 964 ± 10 cm^{-1}) is essentially coincident with the higher energy HHH origin component. A more accurate estimate of band center can be derived indirectly from the position of the sharp high-energy HDH component at 32 090 cm^{-1}, which represents the D origin, shifted about 4 cm^{-1} to the blue (32 086 cm^{-1}) by interaction with the H molecules. (These shifts, which are <7 cm^{-1}, are estimated by using the resonance calculations described in the next section.) The DDD origin band center (32 083 cm^{-1}, Table III) is essentially coincident with this position. This establishes that the upper observed DDD origin doublet component is near the band center. The isotope shift between HHH and DDD clusters is 118 cm^{-1}, based on the difference in measured origin positions for the pure clusters. This shift applied to the corrected position of D in HDH (32 086 cm^{-1}) places the HHH band center at 31 968 cm^{-1}, in excellent coincidence with the upper observed HHH origin component. The vibrational analyses presented in Table III are based on these origin band-center assignments.

The preliminary conclusion from the trimer vibrational analysis is that resonance interaction is negative for the origin, the upper observed component is quite near band center, and the top component is not observed. The weak transition at 32 008 cm^{-1} for HHH corresponds to an intermolecular vibrational mode, which should exhibit negligible resonance interaction in the weak coupling model. The observed spectra corresponding to intramolecular vibrational excitation are in good accord with expectations for transitions with all parallel transitions moments, in that there is one observable component for each nontotally symmetric mode and these components are substantially red-shifted with respect to the monomer. This indicates the resonance interactions are negative, whereas the substantial shifts in vibrational energies, relative to the monomer, for modes ranging from weak to strong in vibronic intensity, indicate there are appreciable shifts of zero-order frequencies in the trimer.

The band intensities of the HDH and DHD origin components are in ratios consistent with the respective isotopic composition. In contrast, the $\bar{8}_0^1$ spectra, shown in Figure 5b, are remarkably different for HDH and DHD. DHD has three well-resolved components. The low-energy component can be associated with H and the high-energy pair of lines may correspond to the D pair of molecules. The positions of these components are close to the corresponding peaks observed in the pure trimers. The $\bar{8}_0^1$ spectrum of the HDH trimer is drastically different from DHD, with only one principal peak (corresponding to H) appearing at low energy. However, the weak transitions, presumably corresponding to intermolecular vibrational modes, are virtually identical for these two species! (Refer to the components marked B, C, E, and G in Figure 5b.) Also, the components marked B, C, and 8 appear at the same wavelength in both HHH and DDD. This provides dramatic confirmation that resonance interaction occurs for the intense dipolar transitions of the monomer and the Franck–Condon effects severely attenuate interactions for the weak transitions,

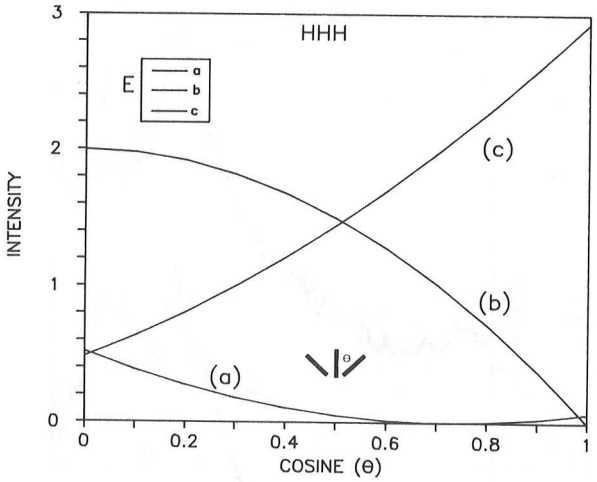

Figure 6. Calculated angular dependence of intensity for excitonic components (a), (b), and (c) of the HHH trimer versus cosine of the angle between adjacent monomer transition moments (i.e., between the long axes of the central and outer molecules). The interactions are assumed to be in the ratios $H_{13} = 0.2$ ($H_{12} = H_{23} < 0$).

leading to the similarities noted above for spectra of different isotopes. Apparently, the HDH wave functions associated with $\bar{8}^1$ cause cancellation of intensity for the expected D component and for the higher energy H components. A description of this intensity effect requires the intensity calculation described in the next section.

2. Trimer Resonance Interaction Calculations. a. Isotopically Pure Trimers. Calculations of transition energies and intensities for HHH and DDD as a function of resonance interaction matrix element $H_{12} = H_{23}$, $H_{13} = 0$ show that each monomer transition splits into three components, located at $+2^{1/2}H_{12}$, 0, and $-2^{1/2}H_{12}$. If intermolecular interactions are negative, the lowest energy component has predominant intensity, whereas the highest energy component has predominant intensity for positive interactions. (For the case with $H_{13} = H_{12} = H_{23}$, two components are degenerate at $-H_2$, and the remaining component has energy $+2H_{12}$; and for intermediate cases of $|H_{13}|$ less than $|H_{12}| = |H_{23}|$, component energies are linearly related to H_{13}. Note that the central component is displaced from bandcenter for nonzero H_{13}.) Calculations were performed for geometries with nonparallel transition moments, as shown in Figure 6, in search of configurations capable of describing observed spectra. (For these calculations the interaction matrix elements were chosen to be constant as a function of intermolecular angle. This choice is not significant for isotopically pure clusters, for which the angle dependence is independent of the magnitude of matrix elements, provided there are no site shifts. However, this is expected to be a crude approximation in the case of mixed isotopes.) There is no assurance that all relevant geometries have been considered, nor that results from the calculations uniquely describe the data. Also, the intensity calculations are insensitive to the positions of molecular centers. Nonetheless, the results are qualitatively useful.

The first conclusion is that short molecular axes are substantially parallel (±25°). If the short axis tilt were larger, a second component would appear for the $\bar{8}_0^1$ transition in the HHH spectrum (Figure 3). Intermolecular interactions are predominately negative, based on the substantially reduced interval observed between the origin and the $\bar{8}_0^1$ component, relative to the monomer frequency. If interactions were positive, the highest energy $\bar{8}_0^1$ component would be observed, and the interval would increase, relative to the monomer. The calculation predicts that the long axis polarized 0,0 transition will have two components of equal intensity, given a cluster geometry as depicted in Figure 7, with long molecular axes displaced at 60-deg intervals. Figure 8 presents dipolar interactions calculated for $\bar{8}_0^1$ as a function of molecular orientation for possible trimer and tetramer structures, assuming an enhanced transition moment. Negative interaction for parallel moments indicates that the molecules are arrayed linearly along the short-axis direction, as shown in Figure 7.

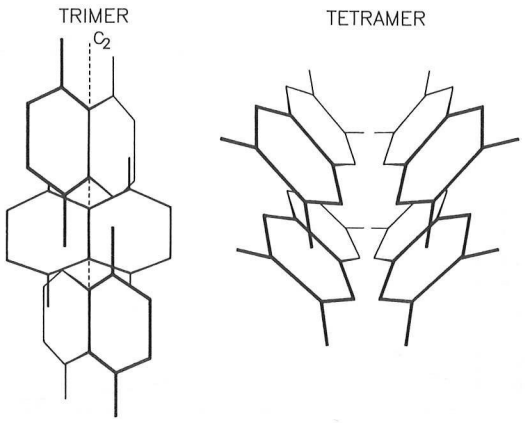

Figure 7. Proposed trimer and tetramer structures. In the trimer, a C_2 axis passes through the central carbons of each molecule, and for the tetramer, the short and normal axes may lie in a mirror plane, with long axes perpendicular to the plane.

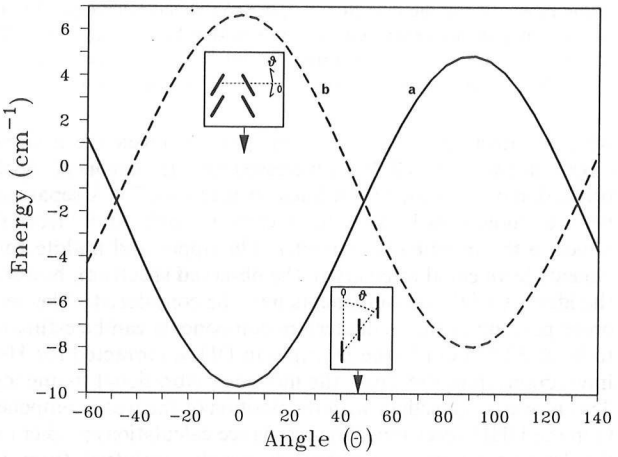

Figure 8. Dipole–dipole pairwise interaction for trimer (a) and tetramer (b) structures. The angular coordinate represents deviation of molecular centers from the configuration depicted at 0°. The transition dipole moment was assumed to be 0.2 D and the intermolecular separation was taken to be 3.7 Å.

Configurations of triangular or pinwheel geometry, with molecular centers in a plane and short axes perpendicular to the plane, are inconsistent with the dipolar model.

If the interactions are scaled to fit the observed separation of the origin components ($H_{12} = H_{23} = -10$ cm^{-1}, $H_{13} = 0.2H_{12}$), then the calculations place the band center 2 cm^{-1} below the highest observed component. This positions the origin band center for HHH at 31 965 cm^{-1}, essentially coincident with the observed H origin in DHD (31 964 cm^{-1}). Based on this deduced HHH origin, the observed $\bar{8}_0^1$ component is displaced 30 cm^{-1} below the monomer frequency. Corresponding displacements of the non-totally symmetric combinations $\bar{8}_0^1 8_0^1$ and $\bar{8}_0^1 7_0^1$ are −17 and −21 cm^{-1}. This is consistent with the expectation that these transitions should be subject to reduced dipolar interactions relative to $\bar{8}_0^1$. These shifts presumably represent significant changes in zero-order frequencies combined with resonance shifts. The displacement of $\bar{7}_0^1$ is anomalously large and probably represents a significant reduction in zero-order frequency of this mode in both HHH and DDD. The transition moment of the totally symmetric mode 8_0^1 is too small to yield appreciable dipolar interaction; thus the −11-cm^{-1} displacement corresponds to a decrease in zero-order vibrational energy relative to the monomer.

We conclude that the model is in good agreement with most of the data. One apparent problem is that the low symmetry of the predicted geometry could be expected to induce site inequivalent interactions, which would tend to increase the number of observed multiplet components. Low symmetry would result in different spectra for the conformers HDH, HHD, DHD, and DDH.

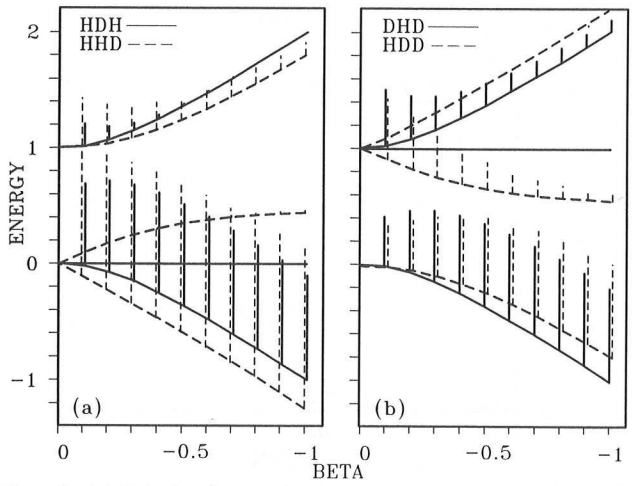

Figure 9. (a) Calculated energy levels (horizontal curves) and intensities (vertical lines) as a function of the interaction scaling parameter β for the HDH trimer (solid lines) and HHD trimer (dashed lines), assuming $H_{12} = H_{23}$, $H_{13} = 0$. (b) Energy levels and intensities for the DHD (solid lines) and HDD (dashed lines) trimers. The results are similar if $H_{12} = H_{23} = H_{13}$. The interaction parameter β and the splitting energy (vertical axis) are expressed in units equal to the zero order separation of H and D (118 cm^{-1}).

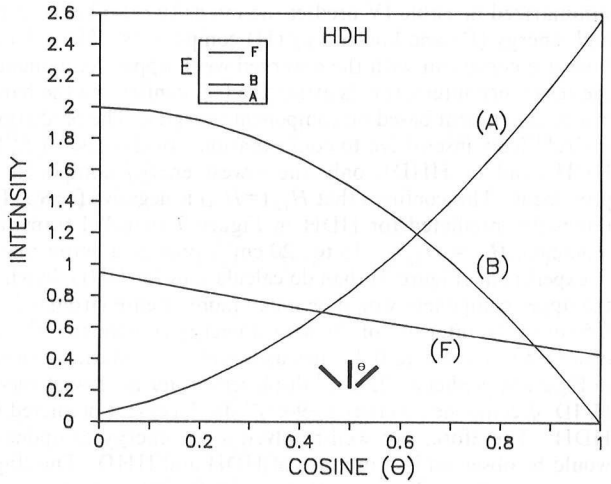

Figure 10. Calculated angular dependence of intensity for HDH trimer with the orientations shown versus cosine of the angle between long axes of the central and outer molecules. The interactions are assumed to be $H_{12} = H_{23} = -20$ cm^{-1}, $H_{13} = -4$ cm^{-1}; however, the results are similar if $H_{12} = H_{23} = H_{13}$. Predictions are independent of the center positions of the monomer units.

TABLE IV: Intensity Ratio for Trimer Origin Components High-Energy Components (D)/Low-Energy Components (H)

		calculated	
cluster	observed	$H_{12} = -15$ cm^{-1}	$H_{12} = +15$ cm^{-1}
HDH	0.2 (+0.1)	0.33	0.70
HHD		0.42	0.57
DHD	1.3 (+0.2)	1.43	3.01
HDD		1.74	2.38

b. Mixed Isotope Trimers. A more detailed analysis of the resonance interactions requires consideration of isotopically mixed cluster spectra. Figure 9 summarizes calculations of intensities and transition energies in HDH, HHD, DHD, and HDD as a function of interaction strength for parallel transition moments, and Figures 10 and 11 present intensity as a function of orientation, for fixed interaction strength. (Table V presents a summary of the interaction parameters derived from the intensity calculations and the vibrational analyses presented here.) The results are generally insensitive to the relative magnitude of H_{13} versus $H_{12} = H_{23}$ and also change little as a function of site shift. We assumed $H_{13} = 0.2H_{12}$, in keeping with approximate expectations for dipolar

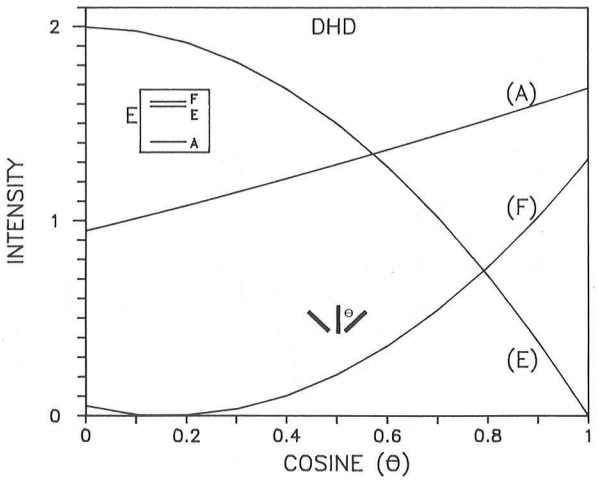

Figure 11. Calculated angular dependence of intensity for DHD trimer with the orientations shown versus cosine of the angle between long axes of the central and outer molecules. The interactions are assumed to be $H_{12} = H_{23} = -20$ cm^{-1}, $H_{13} = -4$ cm^{-1}; however, the results are similar if $H_{12} = H_{23} = H_{13}$. The results are independent of the center positions of the monomer units.

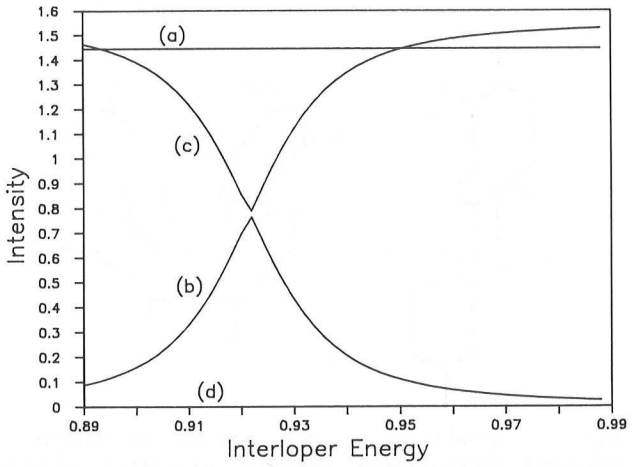

Figure 12. Calculated spectrum for a DHD trimer with three parallel transition moments and a fourth weakly coupled interloper state with no inherent transition moment. The predicted highest component has vanishing intensity and the two intense upper components correspond to the pair of components generated from interaction between the lower DD component and the interloper state. The interloper state corresponds to an intermolecular vibrational addition to the H component.

coupling for the structure shown in Figure 7, and site shifts are neglected. For the HDH (and/or HHD) origin, the calculations summarized in Table IV predict the intensity ratio between the high-energy (D) and low-energy (H) components. The calculations are consistent with the observed weak upper component if the resonance interaction is attractive (−), confirming the band-center assignment based on component energies. The predictions are relatively insensitive to conformation. In the case of $\bar{8}_0^1$ for HDH (and/or HHD), only the lowest energy component is prominent. This confirms that H_{12} ($=H_{23}$) is negative for $\bar{8}_0^1$. The intensities predicted for HDH in Figure 9 (parallel transition moments, $H_{12} = H_{23} = -15$ to -20 cm^{-1}) provide a better match to experiment (Figure 5) than do calculations for HHD, in which the upper component would be much more intense (from 0.25 to 0.5 times the intensity of the lowest energy component) than is observed (from 0.1 to 0.2 times as large). Calculations, shown in Figure 9, predict a −22-cm^{-1} displacement for the lowest energy HHD $\bar{8}_0^1$ component versus a −9-cm^{-1} displacement predicted for HDH. Therefore, two well-resolved lower energy components would be observed in a mixture of HDH and HHD. The single component observed suggests that one conformation predominates and that inequivalent site interactions are less than resonance interactions. (The near coincidence of the lowest energy components of $\bar{8}_0^1$ for DHD and HDH strongly reinforces the argument against the presence of the HHD conformer, because the strong HH interaction for HHD would displace the lowest energy component from the corresponding H component of DHD, as is evident by comparing corresponding components in Figure 9. The angle dependence calculation, shown in Figure 10, predicts the low-energy (HH) components of the HDH origin will be stronger than the highest energy component and that the lowest energy $\bar{8}_0^1$ component will have predominate intensity, as observed. It should be noted that resonance interaction matrix elements exceeding −10 cm^{-1} are required in order to explain the near absence of the highest energy (D) $\bar{8}_0^1$ component in the HDH spectrum. The same calculations predict a shift of +2 cm^{-1} for this component. If the vibrational frequency is unchanged from that of the S_1 monomer (418 cm^{-1}), this would place the component at 32 501 cm^{-1}, which is near the peak labeled G. However, the precise coincidence of G in the DHD and HDH spectra, together with the expectation of a red shift in the zero-order vibrational frequency, suggests that G is associated with an intermolecular vibration and that F is the missing principal component in HDH.

For DHD, the calculation represented by Figure 11 and Table IV predicts that the upper origin components should be slightly stronger than the lowest energy component for attractive resonance interaction, as observed. For $\bar{8}_0^1$, calculations indicate that the lowest energy and highest energy components should be intense, with a vanishing intermediate component, given the assumed dipolar interactions. (If H_{13} is increased from the enhanced dipolar prediction of −2.3 cm^{-1} for a linear trimer with 7.4 Å separation between molecules 1 and 3, to −4 cm^{-1}, intensity shifts from the upper to the middle component.) The upper and middle components have equal intensity in the observed spectrum; however, the identity of these components must be considered. The zero-order position of the $\bar{8}_0^1$ deuterium components can be estimated to be at 32 502 cm^{-1} (the D origin in DHD, corrected for H–D interactions, plus 418 cm^{-1}, the monomer vibrational frequency). This is nearly coincident with the position of the weak component G in the DHD spectrum. The resonance calculations predict that the highest energy component is nearly unshifted from the zero-order position, provided $H_{12} = H_{23} > -20$ cm^{-1}. Both this consideration and the intensity calculations suggest that there is effectively complete intensity cancellation for the highest energy deuterium component, and therefore, that E represents an additional transition.

The additional component may arise from a resonant interloper state, which has no inherent transition moment; however, it interacts with the optically coupled upper state components when its zero-order energy is sufficiently close to resonance with an optically accessible component. This would remove the transition moment cancellation that occurs for the three-level system, resulting in the observed pair of intense upper components, E and F. Intermolecular vibrations added to the H vibrational motion provide potential interloper states. A four-level resonance interaction calculation, shown in Figure 12, was carried out to investigate this possibility. For the case of three DHD levels with parallel short or long transition moments and no site splitting, the DD resonance interaction results in one allowed and one forbidden component, which is in complete agreement with qualitative expectations. When a fourth, interloper level, is added to the calculation, a second intense component is predicted in the region of E and F, and the highest energy component remains essentially forbidden, displaced to a position between peaks F and G. This provides a satisfactory explanation for the three-component DHD spectrum.

An alternative explanation for the DHD $\bar{8}_0^1$ spectrum is that both DHD and HDD conformations contribute. The resonance calculation applied to HDD (Figure 9) is in agreement with the observed origin intensities, and it also predicts similar shifts for the H $\bar{8}_0^1$ components in HDD and DHD. The highest energy component, corresponding to the observed peak F, should be intense for HDD, and the intermediate level should be intense for DHD, corresponding to E. The predicted E–F separation is in agreement with experiment. Therefore, both species may be

TABLE V: Interaction Parameters (cm^{-1})

	trimer						
	HHH	DDD	HDH	DHD	best est	tetramer	crystal
site splitting ($E_{nn} - E_{mm}$)	<5	<5	<5	<5	<2	±30, ±6	0
origin band center (H)	31965	31967	31966			31860	31550[f]
reson interactn							
$H_{12}(0,0)$	−10[a]	−10[a]	∼−15[b]	∼−15	−12	∼15	15[g]
$H_{12}(8^1)$	$-10 > H_{12} > -20$[c]	$-10 > H_{12} > -20$	$-15 > H_{12} > -20$[d]	$0 > H_{12} > -20$	−15	∼20[e]	−8[h]

[a] Measured from origin component splitting. [b] Estimated from origin component intensity ratio. [c] Estimated from energy shift relative to monomer. [d] Estimated by comparing Figure 5b and Figure 9. [e] Estimated by comparing Figure 13 and Figure 15. [f] Estimated from Colson, Hanson, Kopelman, and Robinson. [g] For the pairwise crystal interaction (at 5 Å) which is most similar to H_{12} in the tetramer (from Hansen). [h] For the pairwise crystal interaction (at 6 Å) which is most similar to H_{12} in the trimer (from Hanson).

present in the case of DHD and DDH, whereas only HDH is observed. We offer no explanation for this at present.

Three-level intensity calculations were carried out for alternative geometries, such as a geometry with the long molecular axes oriented with the shape of the letter N. In this case high intensity is predicted for the highest energy HHH origin component, whereas this component is missing in the spectrum. An unlikely H-shaped geometry is required to approximate the observed doublet origin.

On the basis of resonance interaction calculations we conclude that the most plausible description of the interactions require H_{12} of −10 to −20 cm^{-1} for both the origin and $\bar{8}_0^1$ (Table V). The most likely geometry has nearly parallel short axes and long axes arranged with approximately 60-deg displacements. The large magnitude of interaction associated with $\bar{8}_0^1$ indicates that the dipolar force field is enhanced at short ranges. The lack of degeneracy in HHH and DDD origin transitions and intensity predictions for the HDH $\bar{8}_0^1$ transition (not shown for C_3 symmetry in Figure 10) are inconsistent with C_3 symmetry, ruling out geometries such as triangles, pinwheels, or propellers. In addition, the repulsive dipolar resonance interaction expected for $\bar{8}_0^1$ in C_3 structures is also inconsistent with the spectra. (C_3 symmetry would account for site equivalence, and the origin splitting might be rationalized by a pseudo Jahn–Teller type distortion; however, the associated intermolecular vibrational modes are absent from the spectra. Therefore these geometries are rejected.) Currently, the most satisfactory structure is obtained by applying the dipolar model to the $\bar{8}_0^1$ trimer spectra, resulting in the structure depicted in Figure 7, with a C_2 axis intersecting (or nearly intersecting) central carbons of all three naphthalene molecules. The absence of observed site splitting implies that inequivalent interactions are less than 5 cm^{-1} for this geometry.

C. Tetramer. 1. Tetramer Spectra. A single component is observed for the tetramer origin band, in both HHHH and DDDD, as shown in Figure 4. This implies that long naphthalene axes are parallel and that resonance interactions are at least comparable to site shifts. In contrast, $\bar{8}_0^1$ displays the four principal components shown in Figure 13, consisting of two weak low-energy peaks and two intense high-energy peaks. This distribution suggests that short molecular axes are skewed and that the resonance interactions are predominately positive for this mode. D_{2h} symmetry geometries are excluded from consideration by group theory. The higher energy vibrations of b_{3g} symmetry also exhibit four prominent components; however, their intensity distributions differ significantly from $\bar{8}_0^1$. This suggests that site shifts occur in the tetramer, and thus, that a low-symmetry geometry, such as C_s or C_1, is appropriate. In most tetramer b_{3g} bands, the low-energy component has minimum line width and the higher energy components have increased widths. This suggests that intermolecular vibrational relaxation rates vary among the resonance components. (In this case, the upper resonance component is characterized by all positive eigenvector coefficients (a_g), and therefore, the Franck–Condon active a_g intermolecular mode of about 40 cm^{-1} should have the most effective coupling to this component.)

The vibrational analysis of the HHHH cluster is summarized in Table VI. Assuming zero-order vibrational energies are unshifted from the monomer, the tetramer origin is calculated to occur at 31 860 cm^{-1}, such that the observed origin component

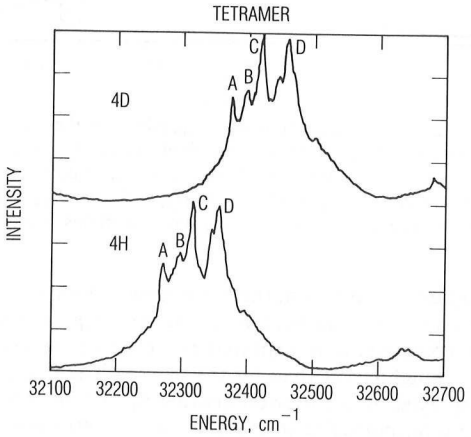

Figure 13. Spectra recorded in the region of $\bar{8}_0^1$ for the HHHH and DDDD tetramers.

TABLE VI

assignt	obsd energy, cm^{-1}	$\Delta\bar{\lambda}$, cm^{-1}	$\Delta\bar{\lambda}$(BC), cm^{-1}	$\Delta\bar{\lambda} - \Delta\bar{\lambda}$(BC), cm^{-1}	$\Delta\bar{\lambda}$(BC) − $\Delta\bar{\lambda}$(monomer)[b], cm^{-1}
		Tetramer, HHHH			
(0,0 BC)[a]	31 860				
0–0	31 903			43	
$\bar{8}_0^1$, A	32 258	398		−37	
$\bar{8}_0^1$, B	32 281	421	435	−14	0
$\bar{8}_0^1$, C	32 301	441		6	
$\bar{8}_0^1$, D	32 340	480		45	
8_0^1	32 617	714[c]			12
$\bar{7}_0^1$, A	32 738	878		−36	
$\bar{7}_0^1$, B	32 767	907	914	−8	
$\bar{7}_0^1$, C	32 780	920		6	3
$\bar{7}_0^1$, D	32 812	952		38	
$\bar{8}_0^1,8_0^1$, A	32 975	1115		−45	
$\bar{8}_0^1,8_0^1$, B	33 017	1157	1160	−3	23
$\bar{8}_0^1,8_0^1$, C	33 033	1173		13	
$\bar{8}_0^1,8_0^1$, D	33 056	1196		36	
$\bar{8}_0^1,7_0^1$, A	33 252	1392		−37	
$\bar{8}_0^1,7_0^1$, B	33 272	1412	1429	−17	2
$\bar{8}_0^1,7_0^1$, C	33 298	1438		10	
$\bar{8}_0^1,7_0^1$, D	33 332	1472		44	
		Tetramer, DDDD			
0,0 BC[d]	31 981				
0–0	32 030	49			
$\bar{8}_0^1$, A	32 359	378		−40	0[e]
$\bar{8}_0^1$, B	32 380	399	418	−19	
$\bar{8}_0^1$, C	32 415	434		16	
$\bar{8}_0^1$, D	32 442	461		43	
8_0^1	32 667	637[f]			0[e]

[a] Calculated, not observed. [b] Shift from monomer vibrational energy. [c] Measured from top component of origin system. [d] Calculated, not observed. [e] Shift from monomer vibrational energy, partly due to resonance interactions. [f] Measured from top component of origin system.

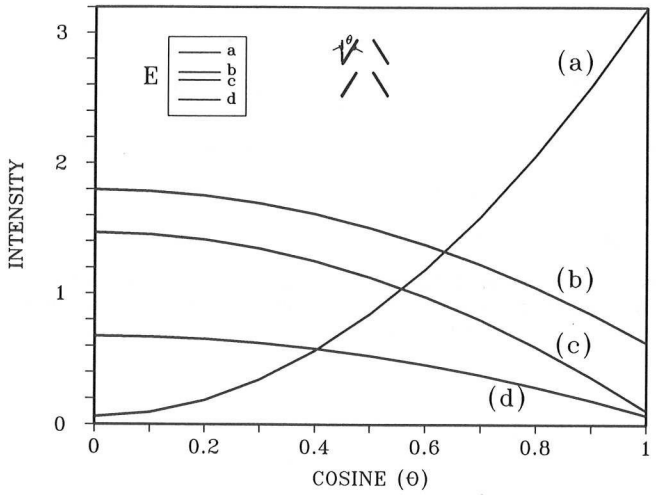

Figure 14. Calculated angular intensity dependence of the low-symmetry, inequivalent site split, HHHH herringbone tetramer structure. Inequivalent site splittings are −30, −6, 6, and 30 cm^{-1} and the interaction parameters are $H_{12} = H_{34} = 18$, $H_{13} = H_{24} = 9$, and $H_{14} = H_{23} = 13$ cm^{-1}. The results are independent of the center positions of the monomer units.

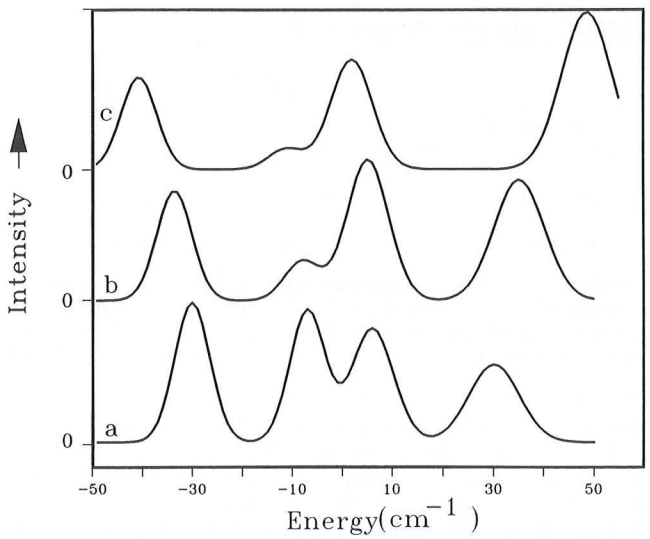

Figure 15. Calculated spectrum for $\bar{8}_0^1$ of HHHH with short axes tilted 37°, using the site splittings and interaction parameters listed in Figure 14. The interaction parameters are reduced by the following factors: (a) 18, (b) 2, and (c) 1.

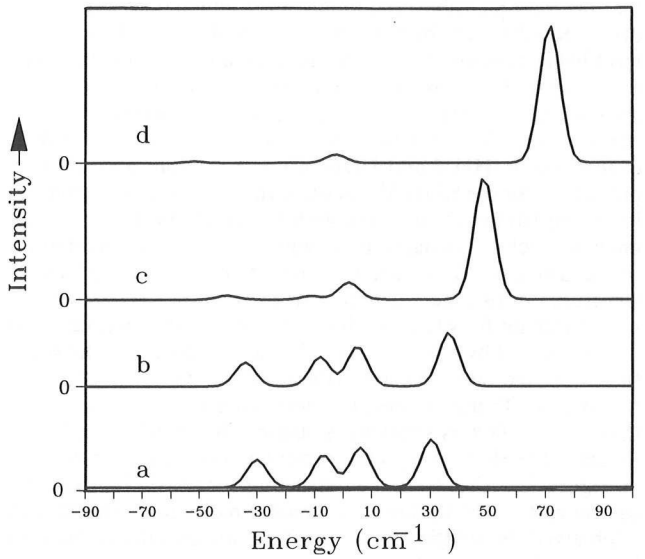

Figure 16. Calculated origin spectrum for HHHH with long axes parallel, with site splittings and interaction parameters listed in Figure 14. The interaction parameters are reduced by the factors (a) 18, (b) 1.8, (c) 1, and (d) 0.6.

is blue-shifted 43 cm^{-1} from the band center. This is the highest energy component, and therefore, the splitting between outer excitonic components is expected to be about 86 cm^{-1}. The splitting is much larger than for the trimer. The 82-cm^{-1} bandwidth displayed by the four observable $\bar{8}_0^1$ components suggests increased intermolecular interaction for the tetramer. Despite the large difference in dipole oscillator strength between the origin, $\bar{8}_0^1$, and higher transitions, they exhibit similar bandwidths. This strongly suggests that a major part of the observed splitting arises from inequivalent site shifted interactions, rather than from resonance interaction. The absence of site-shifted components in the origin band is explained by the resonance interaction calculations described below. The $\bar{7}_0^1$ band exhibits slightly reduced overall bandwidth and greatly altered intensity distribution, as is expected on the basis of a simple dipolar interaction mechanism. The calculated band center at 914 cm^{-1} is equal, within experimental error, to the monomer frequency. On the basis of the similarity of component splitting patterns for each b_{3g} vibrational band, independent of overall intensity, we conclude that inequivalent site interaction dominates the resonance energy shifts for b_{3g} modes and combinations. The appearance of a single principal component for 8_0^1, displaced 720 cm^{-1} above the origin component, suggests that only the highest energy component is observed and that the frequency increases relative to the monomer. The calculated combination frequency for $\bar{8}_8^1$, 8_0^1 is then 1155 cm^{-1}, in good agreement with the observed frequency interval.

Although there is less data for the DDDD tetramer, the results are essentially identical. The origin band center lies 49 cm^{-1} below the first observed component and $\bar{8}_0^1$ displays four components with intensity distribution and displacement energies essentially identical with HHHH. We conclude that the changing intensity patterns for different nontotally symmetric vibrations arise from the interplay of nonequivalent site splitting interactions with vibration-independent resonance interactions.

2. Tetramer Resonance Interaction Calculation. Many degrees of freedom are available in selecting tetramer geometries. We consider the nominal case of parallel long axis monomer transition moments and relatively symmetric cases with tilted short monomer axes. The knowledge that many crystals containing molecules resembling naphthalene tend to have herringbone geometric structures[26] motivated us to emphasize this geometry. A number of structures of C_{2v} and lower symmetry were considered. In each case, an energy matrix was set up, with maximum interaction between nearest neighbors and reduced interactions between more distant neighbors. In the most successful calculations, site shifts were chosen to match the energies of the observed components in the weak $\bar{7}_0^1$ band. Based on the dipolar approximation, resonance interactions should be negligible for this band. Inequivalent site interactions deduced from these components are about −30, −6, 6, and 30 cm^{-1} (Table V). They coincide with qualitative expectations for a low-symmetry herringbone structure, in which the outer molecules have a single near neighbor and thus should have energies shifted significantly from the central molecules, which have two nearest neighbors. The calculations for herringbone geometry, represented in Figures 14–16, predict that the high-energy origin component predominates for a structure with parallel long axes, provided H_{12} (the largest interaction term) for the origin is 15 cm^{-1} or more. The calculations also provide good estimates for the intensity distribution observed for $\bar{8}_0^1$, wherein the second component is extremely weak and the upper two components have predominate intensity. The calculations (Figure 14) predict that the short molecular axes are tilted about 37° and the resonance interaction is about 15 cm^{-1}. Figure 5 predicts how intensity patterns depend on resonance interaction for short axis polarized modes. A four-component structure should be observed for weak transitions, such as $\bar{7}_0^1$, and this should evolve into a three-component structure (as observed in Figure 4), given the

(26) Wyckoff, R. W. G. *Crystal Structures*; Interscience; New York, 1960.

strong resonance interactions of $\bar{8}_0^1$. The dipole interaction parameters used for the trimer were applied to the tetramer $\bar{8}_0^1$ transition. A herringbone structure would have the largest positive interactions for the symmetric configuration shown in Figure 7. The sign of interaction corresponds to experiment and the enhanced transition dipole moment provides a good fit to the data.

Figure 16 predicts the origin spectrum for parallel long molecular axes, as a function of increasing interaction. Observation of a single origin component implies H_{12} is 15 cm^{-1} or larger. This exceeds dipolar interaction terms for the weak origin transition by an order of magnitude, this providing evidence for nondipolar resonance interaction. Nondipolar interactions vanish for nontotally symmetric modes in the Condon approximation. Therefore, resonance interactions for weak transitions, such as $\bar{7}_0^1$, should be negligible. In summary, predictions for a low-symmetry herringbone structure based on a model with inequivalent site splittings is in excellent agreement with the tetramer spectra. The resonance interactions deduced from this model (summarized in Table V) are similar to those observed in the trimer and in the crystals.

V. Summary and Conclusions

The vibronically induced trimer and tetramer spectra are entirely consistent with the weak interaction model, in which the resonance interactions are approximately proportional to the optical transition strengths. In the case of the origin transitions, interactions greatly exceed dipolar coupling, as was observed, but never successfully explained for the crystal origin. These results imply that simple exponential wave functions may underestimate the long-range (nonmultipolar) Coulomb and exchange interactions. For the vibronic transitions, resonance interactions in the clusters exceed dipolar coupling calculated for isolated molecule oscillator strengths and crystalline intermolecular distances. However, the agreement is reasonable, given solvent-type enhancement effects, the considerable uncertainty in the appropriate value for oscillator strength in the reduced symmetry of the cluster, and the possibility of reduced intermolecular separation in the clusters.

The vibrational analysis for the tetramer is compelling and direct, without requiring results from mixed isotopic species. Vibrational frequencies are essentially unshifted from those for the monomer provided resonance interaction effects are taken into account. A low-symmetry herringbone geometry with parallel long molecular axes is consistent with the spectra. This structure, which resembles the crystal unit cell, leads to significant inequivalent site interactions. In contrast, the trimer spectra provide no clear evidence for inequivalent molecular sites. Most of the vibronic transitions have single components, unsplit by site shifts, and the mixed isotope cluster HDH has a single-component principal vibronic transition, which is inconsistent with the existence of substantially different sites, as might be expected for an HHD conformation. However, the origin spectra rule against the high-symmetry geometries that require site equivalence. The simple intensity calculations, combined with a dipolar force field model, suggest the trimer structure shown in Figure 7, which is quite different from the crystal, with nearest-neighbor distances reduced to about 3.5 Å versus 5 Å in the crystal. The small site shifts may be a result of poor geometrical overlap between π-electron systems in the trimer geometry.

The sharp vibronic spectra, with weak intermolecular vibrational participation, indicate that the trimer and tetramer have stable geometries that change little between ground and excited states. In contrast, the prominent spectral broadening observed for the dimer may be caused by large geometry changes and/or dynamical processes in the excited state. The stability of the larger clusters may derive from geometries that hinder excimer formation. The effects of delocalized excitation are apparently not dominant because excimer configurations are not observed in the case of HHD and HDD trimers, which are subject to strongly localized excitation.

Future experiments will probe dynamical processes in naphthalene clusters and extend measurements to larger stable clusters. Studies of isotopic mixed species may provide a more detailed understanding of interactions in the clusters and extension of the method of structural analysis employed here to larger clusters may help to complete the understanding of structural and dynamical properties as they evolve from the monomer to bulk crystal. It will be interesting to discover if the tetramer structure represents an early approach to bulk crystal geometry or if larger clusters assume unrelated shapes. Information from these studies will be useful in supplementing ab initio cluster structure determinations,[9,27] which are currently limited by problems associated with the existence of multiple local potential minima. Clearly, there is need to apply more powerful analytical models to the cluster data in order to test the assumptions involved in this simple analysis and to improve the understanding of long-range intermolecular forces.[28]

Acknowledgment. We acknowledge the excellent technical support provided by Eric Abendroth and financial support provided by the Office of Health and Environment, Department of Energy, grant DE-FG03-86ER60391.

(27) van de Waal, B. W. *Chem. Phys. Lett.* **1986**, *123*, 69; *J. Chem. Phys.* **1983**, *79*, 3948.

(28) Buckingham, A. D.; Fowler, P. W.; Hutson, J. M. *Chem. Rev.* **1988**, *88*, 963.